Dynamical Modelling of the Motorised Momentum Exchange Tether Incorporating Axial Elastic Effects

Yi Chen* Matthew P. Cartmell**

yichen@mech.gla.ac.uk matthewc@mech.gla.ac.uk

Abstract

A discretised planar tether model is proposed for the Motorised Momentum Exchange Tether (MMET) in which axial elasticity is accommodated. The model uses a generalised co-ordinate defining angular motion of the tether about its centre of mass, as it travels at constant velocity on a circular orbit in the Earth's equatorial plane and a generalised coordinate depicting the elastic part of the tether length. The system comprises a symmetrical double payload configuration, with outrigger counter inertia, and it is shown that including axial elasticity permits an enhanced level of modelling accuracy for the tether both in librating and spinning modes. A simulation has been devised in MATLAB and SIMULINK for different data cases. This work will be used later within a spin-up control system and will act as a precursor for an in-depth study into the multi-scale dynamics of MMET tethers and space webs, on more complicated orbits. This, in turn, will be assimilated within new mission architectures.

1 Introduction

The motorised momentum exchange tether (MMET) was first proposed by Cartmell [1] and based broadly on the conceptual schematic of the system shown in Figure 1. The model and concept were developed further, Ziegler and Cartmell [2], which led to proposals by Ziegler [3], who took physical angular co-ordinates for the generalised co-ordinates representing spin and tilt, and a further angular co-ordinate defining back-spin of the propulsion motor's stator components, known henceforth as the outrigger sub-system.

In Figure 2, there are two generalised co-ordinate systems, one is an Earth centred $X - Y - Z$ global co-ordinate system, the other is the $x_0 - y_0 - z_0$ relative rotating co-ordinate system. Two payload masses at each end, M_1 and M_2, are connected by the tether sub-span, where the distance from the tether's centre of mass M_0 to each end mass is denoted by L. R, R_1, and R_2 are the distances from $E(0, 0, 0)$ to $M_0(x_0, y_0, z_0)$, $M_1(x_1, y_1, z_1)$, and $M_2(x_2, y_2, z_2)$, respectively, with $M_1 = M_2 = M_P$, and $M_0 = M_M$. The centre of the Earth is denoted by $E(E_x, E_y, E_z)$, which is

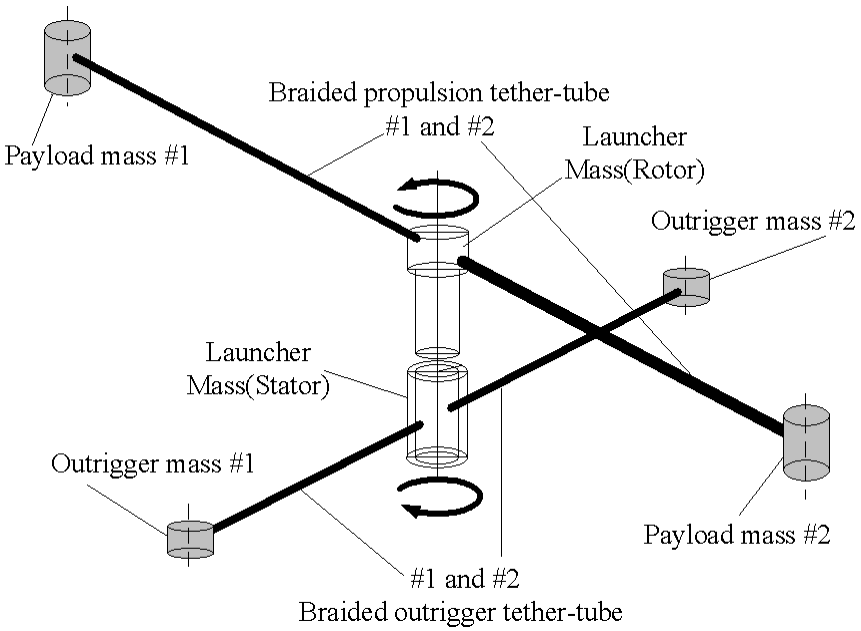

Figure 1: Conceptual Schematic of the Motorised Momentum Exchange Tether

defined as the origin of the $X - Y - Z$ system. The origin of the $x_0 - y_0 - z_0$ rotating system is located at the centre of the facility mass. The $X - Y$ plane and the $x_0 - y_0$ plane lie coplanar to the orbit plane, where the Z and z_0 axes are perpendicular to the orbit plane. The X axis is aligned along the direction of the perigee of the orbit, and the x_0 axis is an extension of R. ψ is the in-plane pitch angle, and this denotes the angle from the x_0 axis to the projection of the tether onto the orbit plane. α is the out-of-plane angle, from the projection of the tether onto the orbit plane to the tether, and is always within a plane normal to the orbit plane. θ is the circular orbit angular position, effectively the true anomaly. In the case of a planar circular orbit, the R , α and θ are constants.

2 Modelling MMET Elasticity

A discretised model of the motorised momentum exchange system is shown in Figure 3. The configuration shown could potentially offer high performance for some design data cases and orbital settings. The model contains both the dumb-bell characteristics, as discussed in previous publications [1] [2] [3], along with new dynamics which are representative of axial elasticity effects. The discretised MMET system comprises a symmetrical double payload configuration, with an outrigger counter inertia, as shown in Figures 1 and 3. The axial elasticity is defined by a string of mass-spring-damper systems, where the masses are connected together serially with springs and dampers, in which, $k_1 = \ldots = k_{N+2}$, $c_1 = \ldots = c_{N+2}$ and $m_1 = \ldots = m_N$. The discretised MMET model in Figure 3 based on a discretisation scheme in which the locations of the point masses along the length of the tether sub-span can be calculated by means of equation (1). The location table of 1 to 20 point masses is given in Figure 4. The location of each point mass within the tether is given by

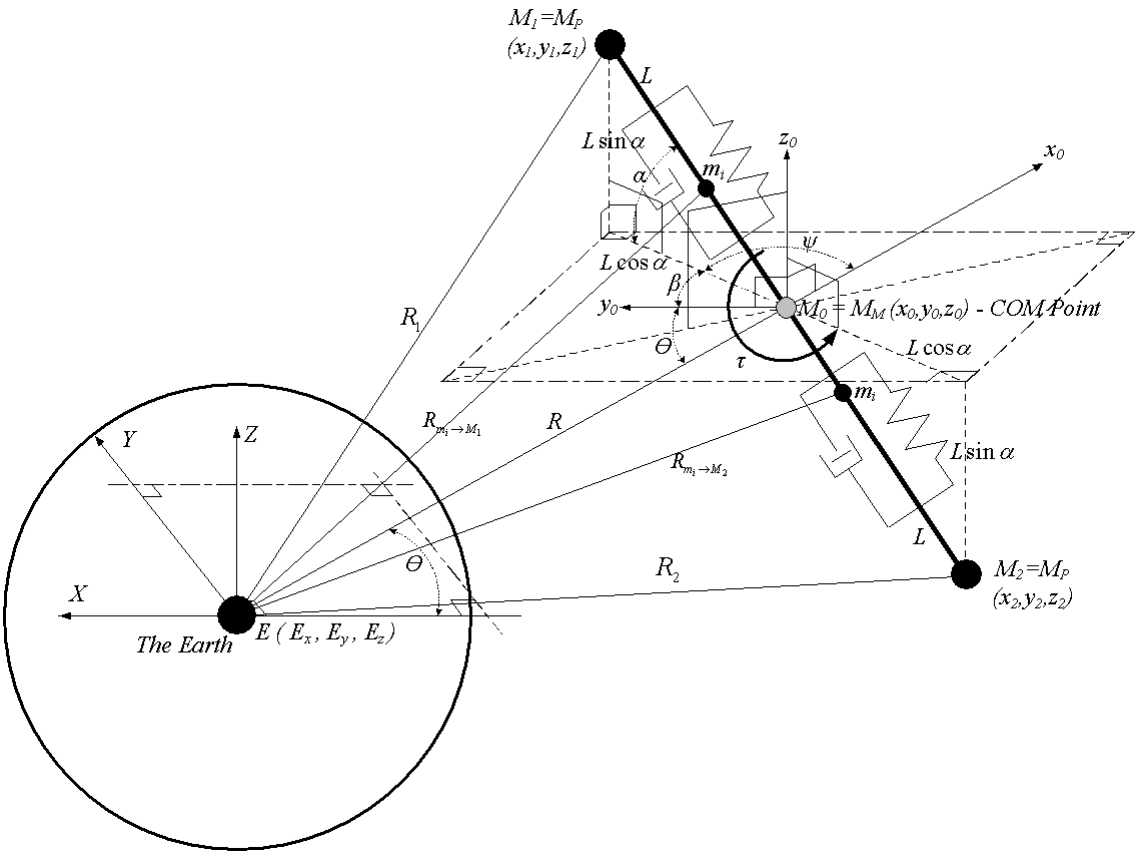

Figure 2: Planar Circular Orbit MMET System Schematic and Coordinates

equation (1):

$$l_i\,(i) = \frac{(2i-1)\,L_T}{2N} \quad (i = 1, 2, ..., N) \tag{1}$$

Figures 3 and 4 show the locations defined by equation (1) for the point masses assumed for modelling the tether. The full length of the tether is L_T in equation (2). L_0 is the original length of each sub-span of the tether when balanced symmetrically, as seen in Figures 3 and 4. The start point is at $i = 0$ on the left, and the end is the L_T point at the right. Figure 4 shows the mass point locations within the full-length of L_T, the values of N in the list are the scaled locations of the point masses along the full length L_T, where N is the number of discrete point masses considered. An example for $N = 2$ is given in Figure 4, where $N = 2$ means there are 2 point masses in the tether, which are located at $0.25L_T$ and $0.75L_T$, respectively. According to previous research [2][3] on the tether's potential energy, there should be at least 15 point masses to approximate adequately the full tether, and so Figure 4 gives a 1 to 20 point mass location scheme. The elastic length of the discretised MMET model is given by equation (3), Δx_i is the relative deformation between two mass points connected directly as defined in equation (7), and the time variant length $L(t)$ of the tether is the sum of the static length, L_0, and the elastic length, L_x, of the discretised tether as given by equation (4).

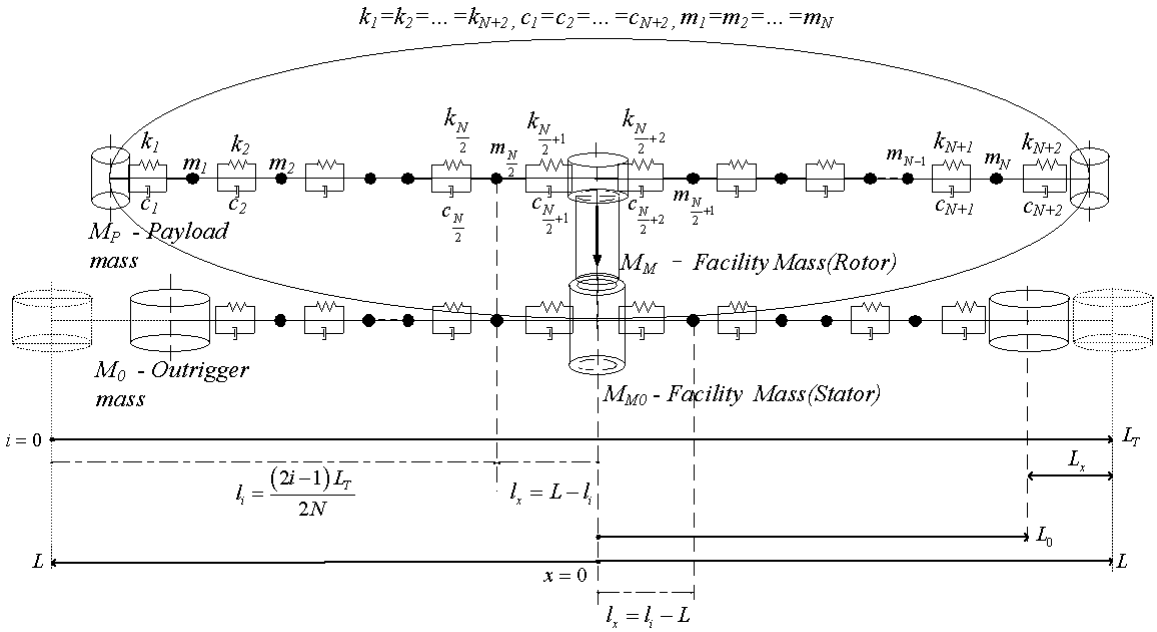

Figure 3: MMET Discretisation Strategy

$$L_T = 2L\,(t) \tag{2}$$

$$L_x\,(t) = \sum_{i=1}^{N+1} \Delta x_i\,(t) \tag{3}$$

$$L\,(t) = L_0 + L_x \tag{4}$$

On this basis equation (1) can be re-written as equation (5),

$$l_i\,(t,i) = \frac{(2i-1)\,L_T}{2N} = \frac{(2i-1)\,(L_0+L_x)}{N} \tag{5}$$

The elastic motion of the symmetrical tether system is considered to be distributed symmetrically along each tether sub-span, and so equation (6) transfers the location of each point mass from the end-point-tether coordinate system, with its generalised coordinate of i from 0 to L_T in equation (5) to the motor-point-tether coordinate system, with its generalised coordinate of x from 0 to L in equation (6). The relative deformation between mass-points m_i and m_{i+1} is given by equation (7), and is also shown in Figure 3 and Figure 5.

$$l_x\,(t,i) = |l_i\,(t,i) - L| = \left|\frac{(2i-1-N)\,(L_0+L_x)}{N}\right| \tag{6}$$

$$\Delta x_i = l_x(t,i+1) - l_x(t,i) \tag{7}$$

In the discretised planar tether model, environmental effects such as solar radiation, aerodynamic drag and electrodynamic forces, that may also influence the modelling, are assumed to be negligible, and the motor consists of a rotor, which is

attached to the propulsion tethers and a stator which can more relative to the rotor by means of a suitable bearing. The power supplies, control systems, and communication equipment are likely to be fitted within the stator assembly in any practical installation. The stator provides the necessary reaction that is required for the rotor to spin-up in a friction free environment. The motor torque is assumed here to remain coplanar with the propulsive tethers and payloads. The tether and the motor are connected by a spring-damper of as in Figure 3, when the tether moves out of the orbital plane, the motor drive axis remains orthogonal to the tether plane, and motor will similarly rotate about its centre of mass. In the planar discretised model, the Cartesian components of the end masses of M_0 , M_1 and M_2 in Figure 2 are given by equation (8),(9) and (10):

$$\left\{ \begin{array}{c} x_0 \\ y_0 \\ z_0 \end{array} \right\} = \left\{ \begin{array}{c} R\left(t\right)\cos\theta \\ R\left(t\right)\sin\theta \\ 0 \end{array} \right\} \tag{8}$$

$$\left\{ \begin{array}{c} x_1 \\ y_1 \\ z_1 \end{array} \right\} = \left\{ \begin{array}{c} x_0 + \left(L_0 + L_x\right)\cos\alpha cos\left(\theta + \psi\right) \\ y_0 + \left(L_0 + L_x\right)\cos\alpha cos\left(\theta + \psi\right) \\ z_0 + \left(L_0 + L_x\right)\sin\alpha \end{array} \right\} \tag{9}$$

$$\left\{ \begin{array}{c} x_2 \\ y_2 \\ z_2 \end{array} \right\} = \left\{ \begin{array}{c} x_0 - \left(L_0 + L_x\right)\cos\alpha cos\left(\theta + \psi\right) \\ y_0 - \left(L_0 + L_x\right)\cos\alpha cos\left(\theta + \psi\right) \\ z_0 - \left(L_0 + L_x\right)\sin\alpha \end{array} \right\} \tag{10}$$

where R,θ, α,ψ, L_x could be defined as independent generalised coordinates, and R, R_1,R_2 are the distances from the Earth's centre to M_0 , M_1 and M_2. R_1 and R_2 are given by equation (11). In the current system, a planar circular orbit model has been chosen and so R ,α and θ are henceforth considered to be constants.

$$\begin{array}{l} R_1 = \sqrt{\left(L_0 + L_x\right)^2 + R^2 + 2\left(L_0 + L_x\right)R\cos\alpha\cos\psi} \\ R_2 = \sqrt{\left(L_0 + L_x\right)^2 + R^2 - 2\left(L_0 + L_x\right)R\cos\alpha\cos\psi} \end{array} \tag{11}$$

$$\begin{array}{l} T = \frac{1}{2}M_P\left(\dot{x_1}^2 + \dot{y_1}^2\right) + \frac{1}{2}M_P\left(\dot{x_2}^2 + \dot{y_2}^2\right) + \frac{1}{2}M_M\left(\dot{x_0}^2 + \dot{y_0}^2\right) + \frac{1}{2}\rho A\left(L_0 + L_x\right) \\ \left(\dot{x}_{T1}^2 + \dot{y}_{T1}^2\right) + \frac{1}{2}\rho A\left(L_0 + L_x\right)\left(\dot{x}_{T2}^2 + \dot{y}_{T2}^2\right) + \left(I_P + I_T + \frac{1}{2}I_M\right)\left(\dot{\psi} + \dot{\theta}\right)^2 \end{array} \tag{12}$$

The discretised planar model is based on aspects of the spin-up of the point-mass planar model, suggested by Ziegler and Cartmell [2] and stated in the results of work by Ziegler [3]. The kinetic energy of a motorised tether, taking into account the translation and rotation of each component, is given by equation (12), and the potential energy is given by equations (13) or (14), incorporating gravitational and elastic strain energy components.

$$
\begin{aligned}
U &= -\frac{\mu M_P}{R_1} - \frac{\mu M_P}{R_2} - \frac{\mu M_M}{R} - \mu\rho A \int_{-(L_0+L_x)}^{(L_0+L_x)} \left(R^2 + l^2 + 2lR\cos\psi\right)^{-\frac{1}{2}} dl + SE \\
&= -\frac{\mu M_P}{R_1} - \frac{\mu M_P}{R_2} - \frac{\mu M_M}{R} + \\
&\mu\rho A \ln\left(\frac{R\cos\psi - (L_0+L_x) + \sqrt{R^2 + (L_0+L_x)^2 - 2(L_0+L_x)R\cos\psi}}{R\cos\psi + (L_0+L_x) + \sqrt{R^2 + (L_0+L_x)^2 + 2(L_0+L_x)R\cos\psi}}\right) + SE
\end{aligned}
\tag{13}
$$

Note that ln() is explicit in equation (13), and that this term has a numerical singularity at $\psi = \mathrm{n}\pi$, which means for the case of a spinning motorised tether problems will be encountered when numerically integrating. To avoid the singularity situation, an alternative description of the potential energy is derived, which discretises the tether mass, and so the potential energy is re-stated by equation (14).

$$
\begin{aligned}
U &= -\frac{\mu M_P}{R_1} - \frac{\mu M_P}{R_2} - \frac{\mu M_M}{R} - \\
&\sum_{i=1}^{N} \frac{\mu\rho A(L_0+L_x)}{N\sqrt{R^2 + \left(\frac{(2i-1)(L_0+L_x)}{2N}\right)^2 + \frac{2(2i-1)R(L_0+L_x)}{2N}\cos\psi}} - \\
&\sum_{i=1}^{N} \frac{\mu\rho A(L_0+L_x)}{N\sqrt{R^2 + \left(\frac{(2i-1)(L_0+L_x)}{2N}\right)^2 - \frac{2(2i-1)R(L_0+L_x)}{2N}\cos\psi}} + SE
\end{aligned}
\tag{14}
$$

The *SE* term is the strain energy of the discretised tether and is defined in equation (16), *CE* is an assumed dissipation function based on Rayleigh damping and defined in equation (17). The mass moments of inertia can be derived from first principles, and are given by equations (15),

$$
I_P = \frac{1}{2}M_P r_P^2, I_M = \frac{1}{2}M_M r_M^2, I_T = \frac{1}{12}\rho A(L_0+L_x)\left(3r_T^2 + (L_0+L_x)^2\right) \tag{15}
$$

where, I_P is the mass moment of inertia of the payload,r_p is the radius of payload, I_T is the mass moment of inertia of the tether,r_T is the radius of the tether, I_M is the mass moment of inertia of the motor, r_M is the radius of the motor.In the discretised model, energy is stored as potential energy in the assumed spring elements. The strain energy for tether elasticity is defined in equation (16).

$$
SE = \sum_{i=1}^{N+1} \frac{1}{2}k_i \Delta x_i^2 = \frac{1}{2}k_{eq}L_x^2 \tag{16}
$$

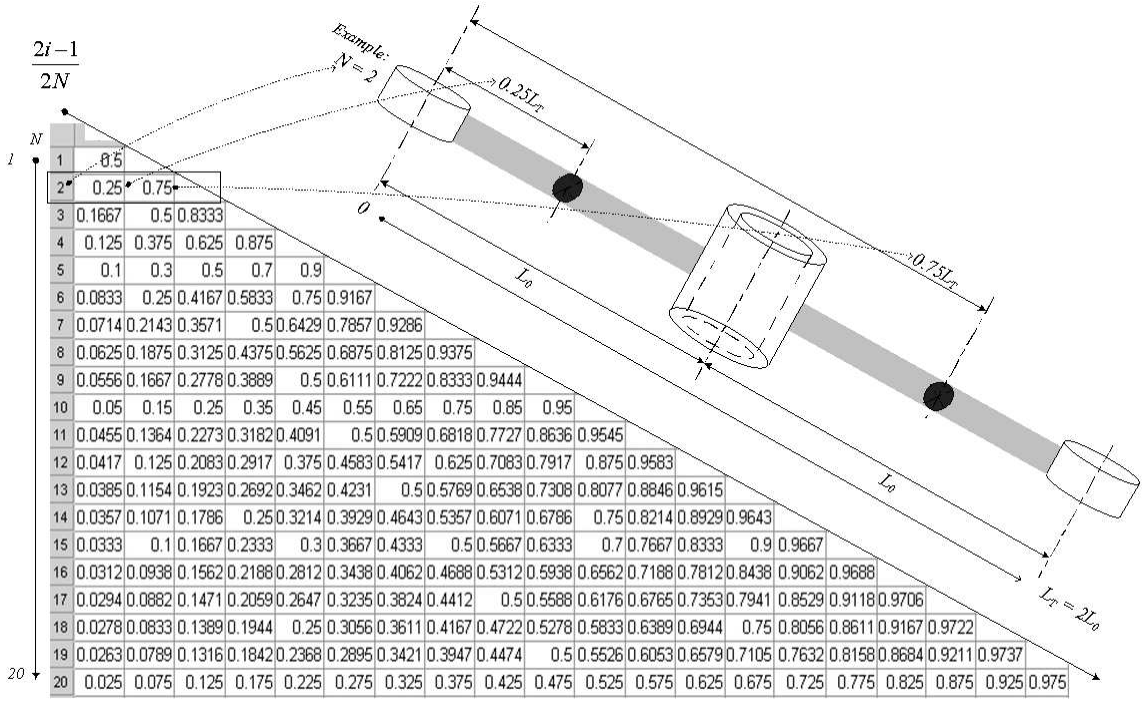

1	0.5																			
2	0.25	0.75																		
3	0.1667	0.5	0.8333																	
4	0.125	0.375	0.625	0.875																
5	0.1	0.3	0.5	0.7	0.9															
6	0.0833	0.25	0.4167	0.5833	0.75	0.9167														
7	0.0714	0.2143	0.3571	0.5	0.6429	0.7857	0.9286													
8	0.0625	0.1875	0.3125	0.4375	0.5625	0.6875	0.8125	0.9375												
9	0.0556	0.1667	0.2778	0.3889	0.5	0.6111	0.7222	0.8333	0.9444											
10	0.05	0.15	0.25	0.35	0.45	0.55	0.65	0.75	0.85	0.95										
11	0.0455	0.1364	0.2273	0.3182	0.4091	0.5	0.5909	0.6818	0.7727	0.8636	0.9545									
12	0.0417	0.125	0.2083	0.2917	0.375	0.4583	0.5417	0.625	0.7083	0.7917	0.875	0.9583								
13	0.0385	0.1154	0.1923	0.2692	0.3462	0.4231	0.5	0.5769	0.6538	0.7308	0.8077	0.8846	0.9615							
14	0.0357	0.1071	0.1786	0.25	0.3214	0.3929	0.4643	0.5357	0.6071	0.6786	0.75	0.8214	0.8929	0.9643						
15	0.0333	0.1	0.1667	0.2333	0.3	0.3667	0.4333	0.5	0.5667	0.6333	0.7	0.7667	0.8333	0.9	0.9667					
16	0.0312	0.0938	0.1562	0.2188	0.2812	0.3438	0.4062	0.4688	0.5312	0.5938	0.6562	0.7188	0.7812	0.8438	0.9062	0.9688				
17	0.0294	0.0882	0.1471	0.2059	0.2647	0.3235	0.3824	0.4412	0.5	0.5588	0.6176	0.6765	0.7353	0.7941	0.8529	0.9118	0.9706			
18	0.0278	0.0833	0.1389	0.1944	0.25	0.3056	0.3611	0.4167	0.4722	0.5278	0.5833	0.6389	0.6944	0.75	0.8056	0.8611	0.9167	0.9722		
19	0.0263	0.0789	0.1316	0.1842	0.2368	0.2895	0.3421	0.3947	0.4474	0.5	0.5526	0.6053	0.6579	0.7105	0.7632	0.8158	0.8684	0.9211	0.9737	
20	0.025	0.075	0.125	0.175	0.225	0.275	0.325	0.375	0.425	0.475	0.525	0.575	0.625	0.675	0.725	0.775	0.825	0.875	0.925	0.975

Figure 4: Point Mass Location Scheme

Damping in each discretised elastic element is assumed to be classical linear viscous in form and is given by,

$$CE = \sum_{i=1}^{N+1} \frac{1}{2} c_i \Delta \dot{x_i}^2 = \frac{1}{2} c_{eq} \dot{L_x}^2 \tag{17}$$

Equation (18) defines the equivalent spring stiffness k_{eq}, and the damping coefficient is c_{eq} for each tether sub-span. A is the tether tube cross-sectional area, stated in equation (19). Also f_0 is the tensile force at the end of each tether sub-span, as defined by equation (20).

$$k_{eq} = \frac{k_i}{N+1}, c_{eq} = \frac{c_i}{N+1} \tag{18}$$

$$A = \pi r_T^2 \tag{19}$$

$$f_i(t) = \dot{\psi}^2(t) \left(M_P + \frac{\rho A \left| \frac{(2i-1-N)(L_0+L_x)}{N} \right|}{2} \right) \left| \frac{(2i-1-N)(L_0+L_x)}{N} \right| \tag{20}$$

In Figure 6 the tether has a payload at each end and rotates due to the motor, thereby experiencing centripetal acceleration. The tether's tensile force related to the tether stress is given by equation (20). Calculating the stress, Ziegler and

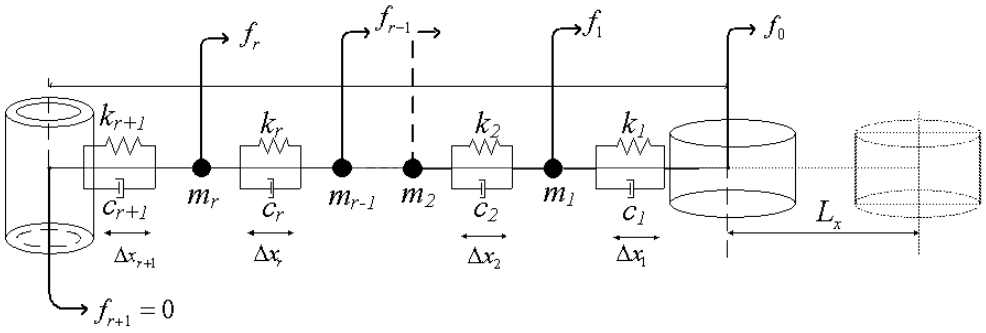

Figure 5: The Relative Deformation Between Mass-points

Cartmell [4], provides a basis for Figure 6 in order to show the stress distribution within the tether sub-spans. This shows the relationship between tether stress, point mass location, and the angular velocity.

It can be note that ψ is defined as the planar pitch angle, and τ is the motor torque, which is assumed to be a constant here. Equations (12), (14) are substituted into Lagrange's equation, leading to the dynamical equations of motion in ψ and L_x.

Since assumptions have been made that there are two non-conservative forces are acting on the system, namely, τ, the motor torque, and Q_{L_x}, the generalised force associated with the generalised coordinate L_x, then a classical linear viscous damping term as a result of assuming a Rayleigh type dissipation function in equation (17) is also assumed in equation (22).

$$\sum_{i=1}^{N} \frac{\mu\rho\pi R r_T^2 (2i-1)(L_0+L_x)^2 sin\psi}{2N^2\left(R^2 - \frac{(2i-1)Rcos\psi(L_0+L_x)}{N} + \frac{(2i-1)^2(L_0+L_x)^2}{4N^2}\right)^{\frac{3}{2}}} -$$
$$\sum_{i=1}^{N} \frac{\mu\rho\pi R r_T^2 (2i-1)(L_0+L_x)^2 sin\psi}{2N^2\left(R^2 + \frac{(2i-1)Rcos\psi(L_0+L_x)}{N} + \frac{(2i-1)^2\,(L_0+L_x)^2}{4N^2}\right)^{\frac{3}{2}}} +$$
$$\frac{1}{6}(\ddot{\theta}+\ddot{\psi})\left(3M_M r_M^2 + 6M_P r_P^2 + 4\pi\rho r_T^2 (L_0+L_x)^3 + 12M_P(L_0+L_x)^2 + 3\pi\rho r_T^4 (L_0+L_x)\right) +$$
$$\frac{1}{6}(\dot{\theta}+\dot{\psi})\dot{L}_x\left(12\rho\pi r_T^2\,(L_0+L_x)^2 + 24M_P(L_0+L_x) + 3\pi\rho r_T^4\right) - \mu R M_P (L_0+L_x) sin\psi$$
$$\left(\frac{1}{(R^2+2R(L_0+L_x)cos\psi+(L_0+L_x)^2)^{\frac{3}{2}}} - \frac{1}{(R^2-2R(L_0+L_x)cos\psi+(L_0+L_x)^2)^{\frac{3}{2}}}\right)$$
$$= \tau \tag{21}$$

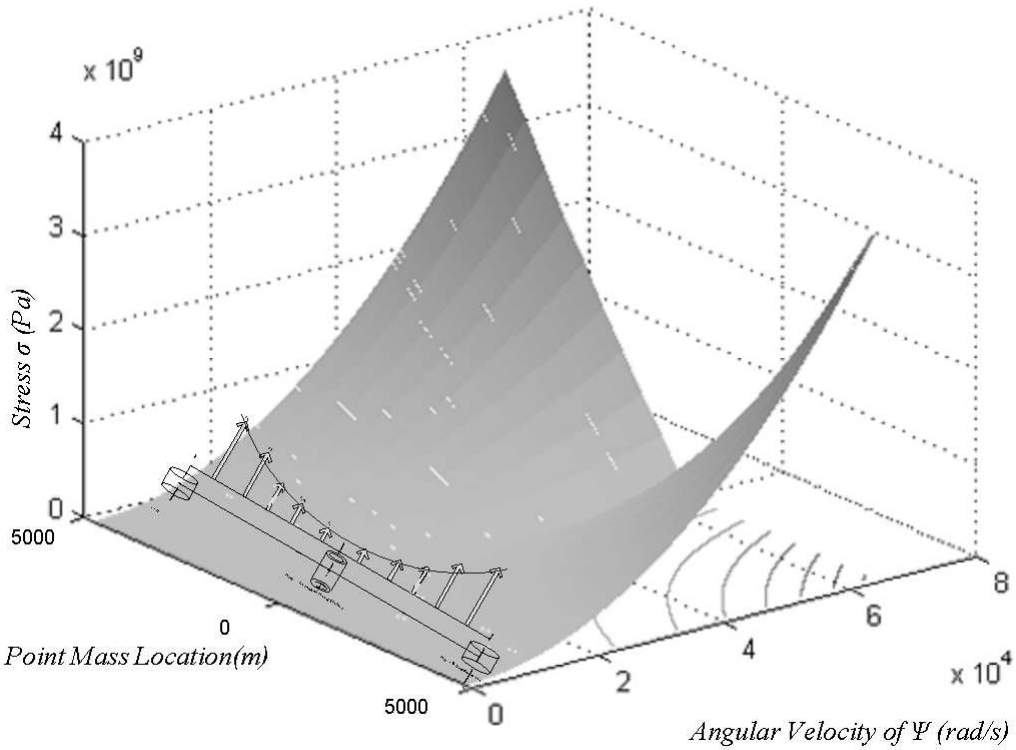

Figure 6: Stress Distribution within Tether Sub-span

$$\left(2M_P+\frac{1}{2}\rho\pi r_T^2(L_0+L_x)\right)\ddot{L_x}+3\rho\pi r_T^2\dot{L_x}-\left(2M_P(L_0+L_x)-\frac{1}{4}\rho\pi r_T^4-\rho\pi r_T^2(L_0+L_x)^2\right)$$
$$\left(\dot{\theta}+\dot{\psi}\right)^2-\rho\pi r_T^2\left(\dot{R}^2+R^2\dot{\theta}^2\right)+\frac{k_0L_x}{N+1}+\mu M_P\left(\begin{array}{c}\frac{(L_0+L_x)-Rcos\psi}{(R^2-2(L_0+L_x)Rcos\psi+(L_0+L_x)^2)^{\frac{3}{2}}}+\\ \frac{(L_0+L_x)+Rcos\psi}{(R^2+2(L_0+L_x)Rcos\psi+(L_0+L_x)^2)^{\frac{3}{2}}}\end{array}\right)$$
$$+\mu\rho\pi r_T^2\left(\begin{array}{l}\sum_{i=1}^{N}\left(\begin{array}{c}\frac{(L_0+L_x)\left(\frac{(2i-1)^2(L_0+L_x)}{2N^2}-\frac{(2i-1)Rcos\psi}{N}\right)}{2N\left(R^2-\frac{(2i-1)Rcos\psi(L_0+L_x)}{N}+\frac{(2i-1)^2(L_0+L_x)^2}{4N^2}\right)^{\frac{3}{2}}}-\\ \frac{1}{N\left(R^2-\frac{(2i-1)Rcos\psi(L_0+L_x)}{N}+\frac{(2i-1)^2(L_0+L_x)^2}{4N^2}\right)^{\frac{1}{2}}}\end{array}\right)+\\ \sum_{i=1}^{N}\left(\begin{array}{c}\frac{(L_0+L_x)\left(\frac{(2i-1)^2(L_0+L_x)}{2N^2}-\frac{(2i-1)Rcos\psi}{N}\right)}{2N\left(R^2+\frac{(2i-1)Rcos\psi(L_0+L_x)}{N}+\frac{(2i-1)^2(L_0+L_x)^2}{4N^2}\right)^{\frac{3}{2}}}-\\ \frac{1}{N\left(R^2+\frac{(2i-1)Rcos\psi(L_0+L_x)}{N}+\frac{(2i-1)^2(L_0+L_x)^2}{4N^2}\right)^{\frac{1}{2}}}\end{array}\right)\end{array}\right)$$
$$+c_{eq}\dot{L_x}=0 \tag{22}$$

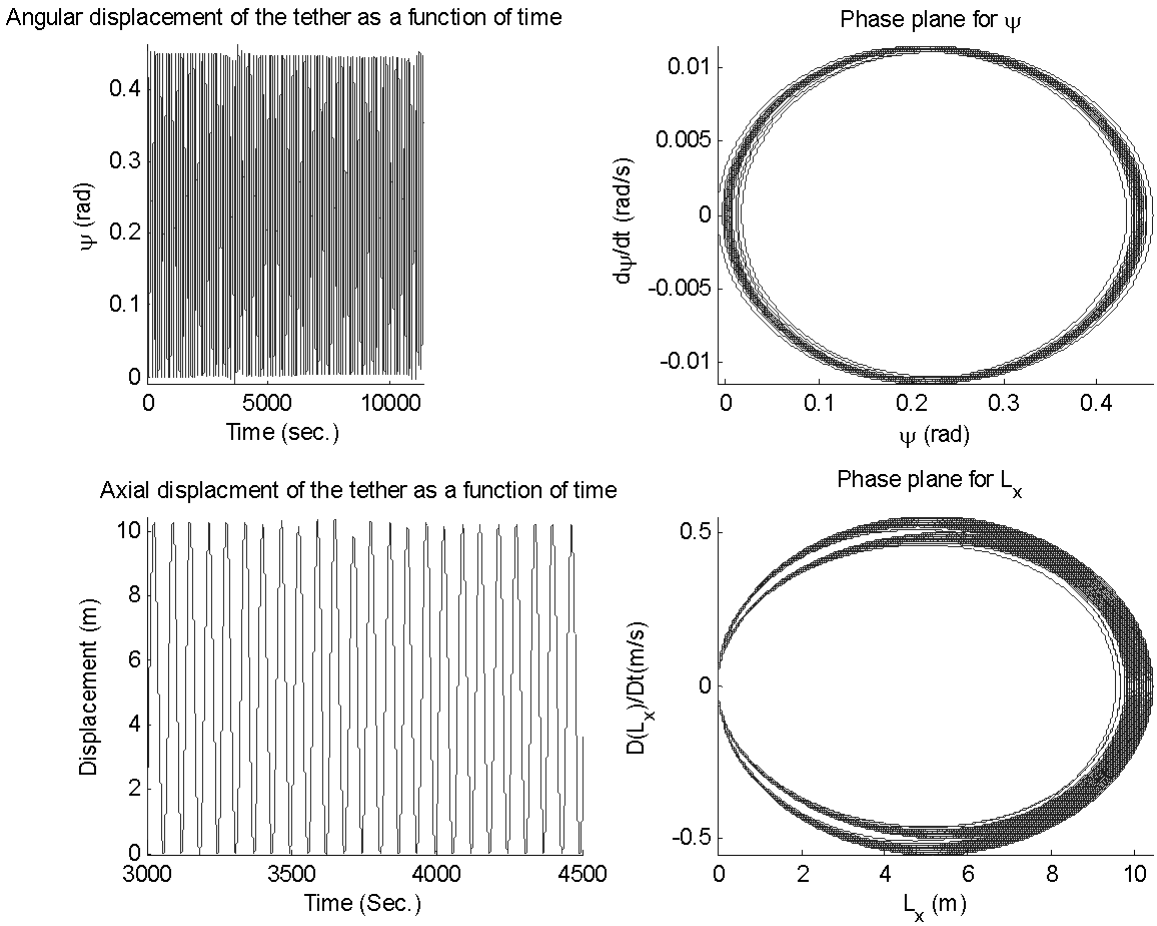

Figure 7: Ψ and L_x Simulation Graphs,$\tau = 2.5 \times 10^8 Nm$

3 Case Study

Unless stated otherwise all of the results were generated with the following system parameters: the number of point masses $N = 20$, gravitational constant $\mu = 3.9877848\times10^{14}\ m^3s^{-2}$, propulsion tether mass of payload $M_P = 1000$ kg, mass of motor facility $M_M = 5000$ kg, static length of propulsion tether $L_0 = 10000$ m, circular orbit with eccentricity $e = 0$, periapsis distance $r_{per} = 6890\ \times10^3$ m, apoapsis distance $r_{apo} = r_{per}$, radius of tether tube $r_T = 0.1$ m, radius of facility of motor $r_M = 0.5$ m, radius of payload $r_P = 0.5$ m, the original tether tube cross-sectional area $A = 62.83\times10^{-6}\ m^2$, the tether density $\rho = 970\ kg/m^3$, initial angular $\psi_0 =$ -0.9 rad, initial angular velocity of $\dot{\psi}_0 = 0.001$ rad/s, motor torque $\tau = 2.5 \times 10^8$ Nm in Figure 7 and $\tau = 2.5 \times 10^12$ Nm in Figure 8, damping coefficient $c_i = 2000$ Ns/m, stiffness k_i= 20000 N/m, acceleration of gravity g = 9.81 m/s^2, The period of elliptical orbit $T = 2\pi(\frac{r_{apo}+r_{per}}{2})^{\frac{3}{2}}/\mu^{\frac{1}{2}}$, Numerical results were obtained by integrating equations (21) and (22), in MATLAB/SIMULINK with a fourth-fifth-order Fehlberg Runge-Kutta method using a relative error of 10^{-6} .

Figure 7 shows the time responses for the pitch angle ψ, and the axial displacement of the tether, L_x, along with their corresponding phase spaces. It is clear that over the integration time shown both quantities exhibit what looks to be steady

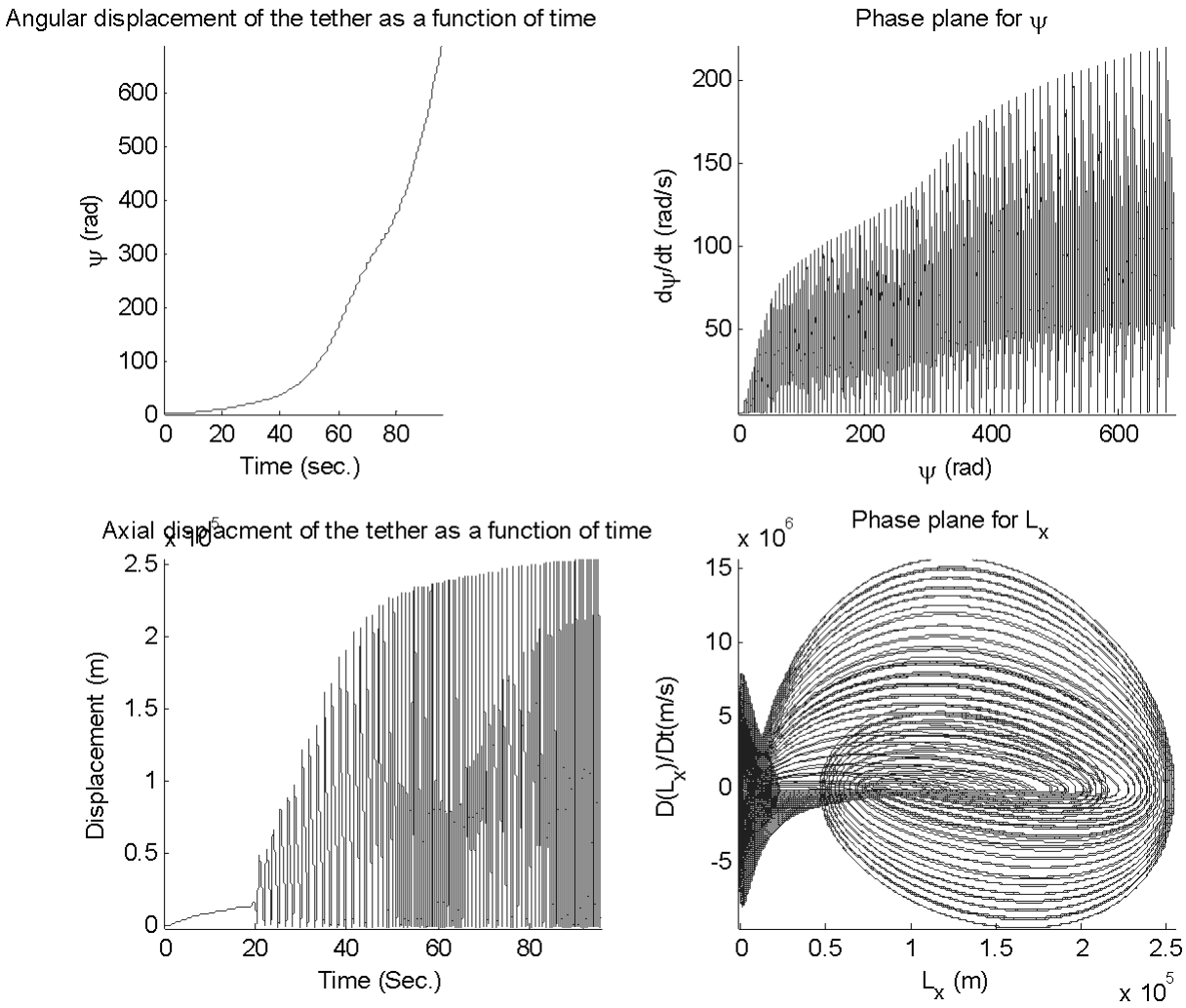

Figure 8: Ψ and L_x Simulation Graphs,$\tau = 2.5 \times 10^{12} Nm$

state oscillation. Physically this equates to libration of the tether, and an axial oscillation about a constant tensile offset from the nominal length of around 5 metres, with an amplitude of approximately +/- 5 metres about that offset value. For an unstretched 10 km sub-span the constant offset represents a stretch of 0.05%, so with the oscillation superimposed on this the tether oscillates between the nominal unstretched length and a maximum extension of 0.1%. This is agreeably small in percentage terms but could still have practical implications for payload delivery and retrieval should the tether be required to work in the librating mode. The phase plots show limit cycle behaviour for each coordinate, which tends to corroborate the interpretations of steady-state. Figure 8 illustrates the system responses once the tether pitch angle has bifurcated out of the periodic libration and into monotonic spin. This response is highly nonlinear but shows a good build-up of rotation in a short time. The axial response shows a gradual growth in tensile stretch over a fraction of a metre and then oscillation once again, about a small tensile offset value of just over 1 m. Although the integration time shown is limited it looks as though the axial coordinate could, in time, reach a steady-state oscillation. How-

ever, the phase plot for the axial coordinate is harder to decipher and a longer time is needed to get accurate clarification of the qualitative aspects of this response. It is interesting to note that the frequency of axial oscillation in Figure 8 is very much higher than that of Figure 7, which is one reason why the plots in Figure 8 are for a shorter integration time, noting that all detail would otherwise be lost. The torque is increased 10000 times to provide the bifurcation from the case of Figures 7 to that of Figure 8.

4 Conclusions

The work in this paper has shown that including axial elasticity within an MMET model has a significant bearing on overall performance and that this effect should not be ignored in future, particularly for control. All subsequent analyses for control applications will henceforth include axial compliance within the modelling.

Acknowledgements

The authors would like to acknowledge the support provided to the first author by the Overseas Research Students Awards Scheme and the Scholarship awarded by the University of Glasgow's Faculty of Engineering.

References

[1] M. P. Cartmell, (1998), "Generating Velocity Increments by means of a Spinning Motorised Tether", 34th AIAA/ASME/SAE/ASEE Joint propulsion Conference and Exhibit, Cleveland Conference Centre, Cleveland, Ohio, USA, AIAA-98-3739.

[2] Ziegler, S.W., and Cartmell, M.P., (2001), "Using Motorised Tethers for Payload Orbital Transfer", Journal of Spacecraft and Rockets, 38 (6), November / December, pp 904-913.

[3] Spencer Wilson Ziegler, (2003), "The Rigid-body Dynamics of Tethers in Space", PhD Dissertation, Department of Mechanical Engineering, University of Glasgow.

* Postgraduate student ** Professor

Department of Mechanical Engineering, University of Glasgow, Glasgow, G12 8QQ, Scotland, UK.